Tailor-Made Quantum Dot and Iron Oxide Based Contrast Agents for *in Vitro* and *in Vivo* Tumor Imaging

Elmar Pöselt,[†,*] Christian Schmidtke,[†] Steffen Fischer,[†] Kersten Peldschus,[§] Johannes Salamon,[§] Hauke Kloust,[†] Huong Tran,[†] Andrea Pietsch,[†] Markus Heine,[‡] Gerhard Adam,[§] Udo Schumacher,[‡] Christoph Wagener,[⊥] Stephan Förster,[¶] and Horst Weller[†,*]

[†]Institute of Physical Chemistry, University of Hamburg, Grindelallee 117, 20146 Hamburg, Germany, [‡]Institute of Anatomy, [§]Department of Diagnostic and Interventional Radiology, and [⊥]Department of Clinical Chemistry/Central Laboratories, University and Medical Center Hamburg-Eppendorf, Martinistraße 52, 20246 Hamburg, Germany, and [¶]Institute of Physical Chemistry I, University of Bayreuth, Universitätsstraße 30, 95447 Bayreuth, Germany

ABSTRACT

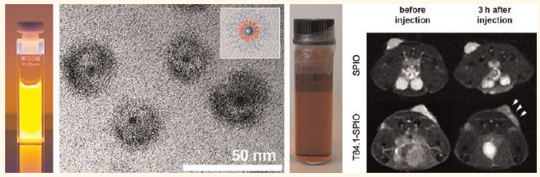

The biofunctionalization of CdSe/CdS/ZnS quantum dots and Fe_3O_4 nanocrystals using a novel ligand system based on polyisoprene-*block*-poly(ethylene oxide) ligands is described. The synthesis includes a partial ligand exchange of the hydrophobic nanocrystals with amino-functionalized polyisoprene ligands, followed by seeded micelle formation of the diblock-copolymers in water. The resulting water-soluble quantum dots showed fluorescence quantum efficiencies in the 40 to 50% range and extraordinary fluorescence stability in the biological environment after cross-linking of the polyisoprene moiety of the ligand shell. No toxicity was detected by water-soluble tetrazolium (WST8) and lactate dehydrogenase (LDH) assays, even at very high nanoparticle concentrations, and almost no nonspecific cell adhesion was detected. The ligand shell was further coupled to the antigen-related cell adhesion molecule (CEACAM) specific monoclonal antibody T84.1. The so-conjugated Fe_3O_4 nanocrystals allowed *in vitro* and *in vivo* tumor targeting by magnetic resonance imaging.

KEYWORDS: nanocrystal · quantum dots · SPIO · biofunctionalization · amphiphilic polymers · PEG · MRI

The use of fluorescent quantum dots (QDs) and superparamagnetic iron oxide nanocrystals (SPIOs) for *in vitro* and *in vivo* imaging in medicine is one of the most competitive fields in modern nanoscience.

These applications require water solubility and high stability of the nanoparticles in the aqueous biological environment.[1] Most advanced preparation techniques for QDs and SPIOs with outstanding fluorescence quantum yields and high relaxivities for magnetic resonance imaging (MRI) are performed in high-boiling organic solvents using hydrophobic ligands.[2,3] Various concepts are described in literature to achieve water solubility, including ligand exchange or encapsulation techniques.[4−9] To achieve biocompatibility of purely synthetic nanocomposites, the outermost ligand moiety usually consists of poly(ethylene oxide) ((PEO), also named polyethylene glycol (PEG)) oligomers or polymers, which are known to exhibit extraordinary degrees of resistance against unspecific protein adsorption.[10] Other concepts are based on loading natural transport vehicles with hydrophobic nanocrystals, as was recently impressively shown for SPIO- and QD-labeled phospholipid nanosomes.[11] The latter concept is, however, limited to imaging of processes associated with fat metabolism.

The purely synthetic approaches, on the other hand, often do not exhibit the required degree of stability and biological inertness for specific targeting of tissues, especially under *in vivo* conditions. Typical problems arise from the insufficient binding strength of the water-soluble nanoparticle ligands under biological conditions, that is, high salt concentrations and the presence of serum proteins, which may either bind nonspecifically to the outermost ligand shell or may even substitute the particle ligands. An additional requirement for tissue targeting is the presence of functional groups at the outermost ligand moieties to allow bioconjugation to target specific molecules, such as antibodies, peptides, or sugars. Closely related to the mentioned structural changes, the nanocrystals may loose their outstanding physical properties in the biological environment. A typical example is the often-observed

* Address correspondence to weller@chemie.uni-hamburg.de, elmar.poeselt@chemie.uni-hamburg.de.

Received for review January 25, 2012 and accepted March 30, 2012.

Published online March 30, 2012
10.1021/nn300365m

drop in photostability and fluorescence quantum efficiency of QDs.

Herein, the synthesis of a new ligand system with outstanding physical and biological properties is reported. It is based on the combination of an amino-functionalized poly(isoprene) preligand (PI-N3) and a polyisoprene-*block*-poly(ethylene oxide) diblock copolymer (PI-*b*-PEO), which results in excellent water solubility and bioinertness of the nanocrystals. The preparation of the final biolables is performed *via* self-assembly processes of the amphiphilic diblock copolymers leading to micelle structures, in which the PI moiety is subsequently cross-linked. Converting the intrinsic outermost hydroxyl functionality of PEO into carboxylate allows easy coupling to a target specific antibody, that is, in this report, the monoclonal T84.1. Furthermore, stability studies as well as toxicity investigations will be presented. Finally, *in vitro* and *in vivo* MRI experiments clearly proved specific binding of the antibody-labeled SPIOs to antigen-related cell adhesion molecule (CEACAM) expressing tumors.

Experimental Section. A detailed description of the block-copolymer synthesis, coupling reactions and spectroscopic characterization is given in the Supporting Information.

RESULTS AND DISCUSSION

Synthesis of Biocompatible Nanoparticles. For these studies, CdSe/CdS/ZnS core−shell−shell and Fe_3O_4 nanocrystals were used, which were synthesized in high boiling organic solvents using trioctyl phosphine (TOP), trioctyl phosphine oxide (TOPO), hexadecyl amine (HDA), and oleic acid (OAc) as ligands *via* well-established literature procedures.[2,3]

A two-step strategy for biofunctionalization of the nanoparticles was employed. In the first step, ligand exchange with 2,2′-diaminodiethylamine-*block*-polyisoprene (PI-N3) in chloroform was performed (I in Scheme 1). PI-N3 was synthesized by coupling polyisoprene to 2,2′-diaminodiethylamine (N3) by CDI activation.[12] PI-N3 serves, on the one hand, as an organic passivator for the trap states in quantum dots, resulting in higher quantum yields, and, on the other hand, as seed for the following micelle formation (for more information see Supporting Information Figure S4). Additional hydrophobic ligands, which are still present from the synthesis, are not prejudicial. Size histograms from dynamic light scattering (DLS) experiments prior and after ligand exchange as well as a TEM image of the ligand exchanged quantum dots are shown in Figure 1. As expected, increases in the hydrodynamic diameter of the particles by 2.1 and 5.2 nm for PI_{30}-N3 (30 isoprene units) and PI_{60}-N3 (60 isoprene units), respectively, were observed. The results also clearly show that no aggregation or clustering of the particles occurred. After ligand exchange chloroform was evaporated and the PI-N3 stabilized

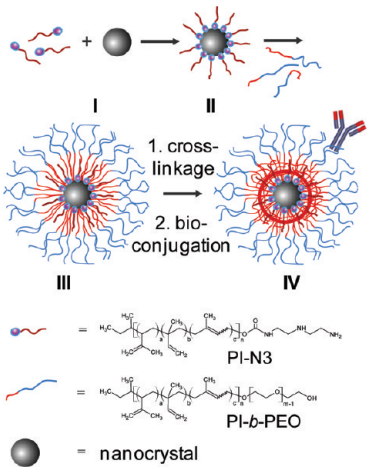

Scheme 1. Illustration of nanoparticle transfer from organic solvents into water and coupling to target specific biomolecules.

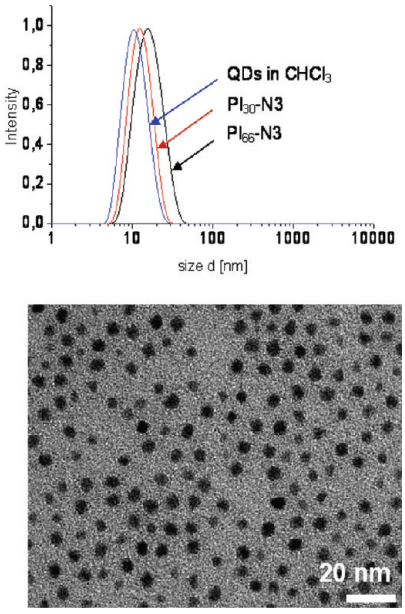

Figure 1. Dynamic light scattering (DLS, intensity distribution) of the as prepared (blue), PI_{30}-N3 (red) coated and PI_{66}-N3 (black) coated CdSe/CdS/ZnS quantum dots in chloroform and the corresponding TEM image of the PI_{30}-N3 coated CdSe/CdS/ZnS quantum dots.

nanoparticles (II) were dissolved in tetrahydrofuran (THF).

In the second step, the amphiphilic polyisoprene-*block*-poly(ethylene oxide) blockcopolymer (PI-*b*-PEO) and a radical initiator azobisisobutyronitrile (AIBN) in THF were added. Briefly, the PI block was synthesized by anionic polymerization and contained mainly of 3,4- and 1,2-isoprene isomer units with terminal −C═C− double bonds. The trans 1,4-isomer was also present, due to the polymerization in THF.[13] Subsequently, the PEO block was synthesized *via* anionic ring-opening polymerization using PI as a macroinitiator. Details of PI-N3 and PI-*b*-PEO syntheses are described in the Supporting Information. The THF solution was then

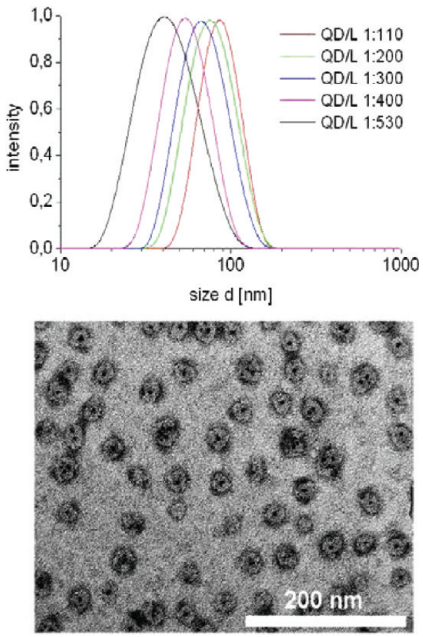

Figure 2. Dynamic light scattering (DLS, intensity PSD) of PI-N3− and PI-*b*-PEO−OH-coated CdSe/CdS/ZnS particles in water and a phosphotungstic acid-stained TEM image of a sample with a hydrodynamic diameter of 55 nm. The sample was purified by sucrose gradient centrifugation and high-performance liquid chromatography (HPLC).

injected into water, where spontaneous self-assembly of the PI-*b*-PEO around the hydrophobic PI-N3 coated nanoparticles occurred under micelle formation (III). The hydrophobic radical initiator was coencapsulated during this process. In the final step, the terminal −C═C− double bonds of the PI blocks were cross-linked *via* thermal radical polymerization (IV). The final size of the micelles could be adjusted by the particle to PI-*b*-PEO ratio during transfer to water. As seen in Figure 2, the hydrodynamic diameter increased from 30 to 40 nm to about 100 nm on decreasing the amount of PI-*b*-PEO from 1:530 to 1:110 QD/L.

To separate the encapsulated nanoparticles from empty micelles, which may also be formed during transfer to water, sucrose gradient centrifugation for the quantum dots or a magnetic column separation in the case of iron oxides were applied. The TEM image in Figure 2 shows the final encapsulated particles with a hydrodynamic diameter of 55 nm. To visualize the polymer shell, the sample was stained with phosphotungstic acid. As can be readily seen, the structure of the cross-linked micelles was conserved even under the high vacuum conditions in the microscope and each micelle carried just one nanoparticle, in most cases. It should be mentioned that this strongly depended on the mixing conditions during transfer to water and that also situations could be achieved in which, on average, more than one particle are encapsulated in each micelle. It is also recognized that the TEM size (25 nm) is only half that obtained from DLS measurements (55 nm). This difference is attributed to

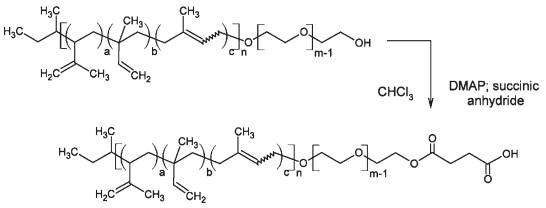

Scheme 2. Generation of a carboxylic functionality at the PEO segment of PI-*b*-PEO−OH by the reaction of the hydroxylic group with succinic anhydride in the presence of 4-dimethylaminopyridine (DMAP) in chloroform.

the strong hydration of the PEG shell in water. Indeed each ethylene oxide unit can be solvated by 2−3 water molecules,[14] which results in a large radius of gyration and a repulsion between the PEO-chains. In fact, Roberts *et al.*[15] reported that the hydrodynamic diameter of PEO is 5−10 times larger than that of a protein with identical molar mass.

The PEO-block of the as-prepared block-copolymer was terminated by just one hydroxyl group. This allows the straightforward attachment of a multiplicity of functional groups, using common functionalization strategies for PEO.[16,17] In this work, the hydroxyl group was modified to yield a carboxylic group *via* reaction with succinic anhydride in the presence of 4-dimethylaminopyridine (DMAP), which acts as a Steglich-Höfle catalyst for the nucleophilic ring-opening reaction (Scheme 2). The corresponding spectra obtained by nuclear magnetic resonance spectroscopy (NMR) and infrared spectroscopy (IR) are shown in Figure S2 (Supporting Information).

Carboxylic groups are chelating agents, which, for example, can interact with magnetite surfaces. In this case, the hydrophobic, cross-linkable PI-segment and the prior encapsulation in PI_{30}-N3 are advantageous because the hydrophilic PEO segment is always exposed to the aqueous phase and an interaction of the carboxylate with the nanoparticle surface is prevented by the PI segment.

OH- and COOH-terminated PI-*b*-PEOs could be mixed in any ratio for micelle formation, allowing control of the average number of coupling groups for 1-ethyl-3-(3-dimethylaminopropyl) carbodiimide (EDC)/*N*-hydroxysulfosuccinimide (sulfo-NHS) coupling to, for examples, antibodies (see below).

Fluorescence and Stability in Aqueous Media. The absorption and fluorescence spectra of the quantum dots in $CHCl_3$ and after transfer into water are shown in Figure 3. There is almost no observable spectral shift, which is attributed to the fact that the local environment of the QDs did not change significantly during the phase transfer into water, since they remain in the hydrophobic micelle core. It is seen, however, that the fluorescence intensity was decreased in water. By optimizing the phase transfer to water (rigorous mixing), fluorescence quantum efficiencies in water in the 40−50% region were obtained. This drop of

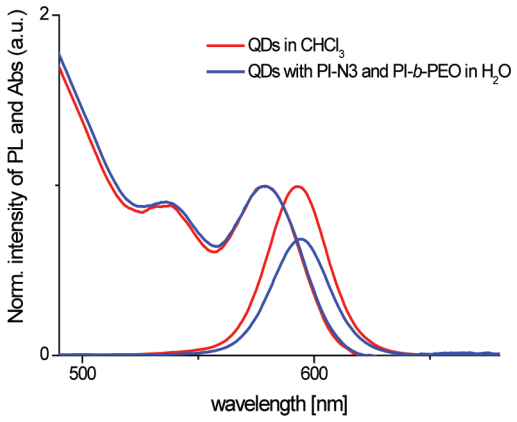

Figure 3. Absorption and fluorescence spectra of the QDs in $CHCl_3$ and after transfer into water.

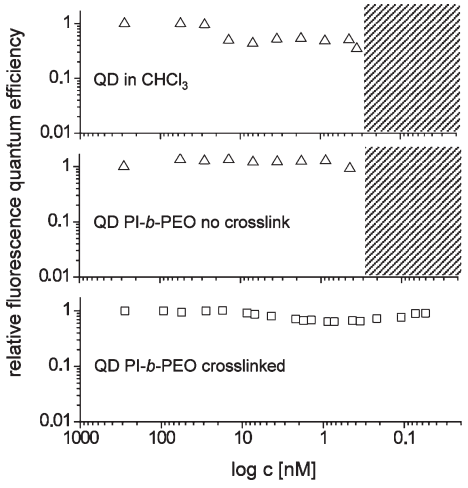

Figure 4. Normalized fluorescence of the QDs upon dilution with $CHCl_3$ and water, respectively: (top) as-prepared QDs; (middle) after transfer into water but without PI cross-linking; (bottom) with cross-linked PI moieties. Owing to the beginning of particle dissolution and colloidal destabilization, no values could be determined within the shaded areas.

quantum efficiency occurred already upon transfer to THF, prior to micelle formation in water.

To further test the QDs for their use as biolables, their stability against dilution and long-term stability in various media were investigated. One of the essential requirements is that the ligand shell is tightly bound to the particles. Organic ligands are, however, typically not bound covalently to the surface of the particles, but underlie a surface equilibrium, which is shifted toward free ligands upon dilution. On the other hand, fluorescence is a very sensitive measure for changes in the ligand shell and thus, a simple dilution experiment gives valuable information about the stability of the ligand shell. The results of these experiments are shown in Figure 4 for the as-prepared QDs in $CHCl_3$ (upper part) and for those after phase transfer to water with and without cross-linking of the PI block (middle and lower part, respectively). Here, the relative fluorescence quantum efficiencies, which were determined by dividing the measured fluorescence intensity by the amount of light absorbed at the respective degree of dilution using the Lambert–Beer Law, are plotted. If the ligand shell remains intact, these values (normalized to 1 at the highest concentration) should not change upon dilution. In other words, the whole construct of QD and ligand shell behaves like a "normal" molecular species in photochemistry, where no concentration-dependent side reaction to fluorescence occurs. This situation is fulfilled down to a particle concentration of 14 nM for the as-prepared QDs, down to 0.3 nM for the non-cross-linked ones, whereas the cross-linked particles were stable down to 50 pM. This value has to be treated as the lower limit of dilution stability, since the sensitivity of the employed spectrometer (Spex Fluorolog 2) reached its detection limit even at largest available slits. The absorbance values of these samples were below 10^{-5}. In the concentration region of the shaded areas of Figure 4, the fluorescence spectra first broaden and shift and then completely fade away with time or upon further dilution, indicating dissolution of the ligand shell. It should be mentioned that identical tests were performed with a series of commercially available water-soluble QDs from reputable suppliers and also with QDs prepared with typical low molecular weight ligands, such dihydroliponic acid. The very best sample was comparable to the non-cross-linked PI-*b*-PEO particles. More detailed comparative surface binding studies of ligand systems will be reported elsewhere. Whereas the QDs in $CHCl_3$ already showed a decrease in quantum efficiency in the 10 nM regime, micelle formation of the amphiphilic block-copolymers gave remarkable stability, but the ultimate performance could only be attained by additional cross-linking within the ligand shell.

To further determine the rigidity of the ligand shell, long-term stability tests in different aqueous solutions were accomplished. For these experiments, very small, green emitting CdSe/CdS/ZnS QDs with a core diameter of <4.0 nm were intentionally used because they are intrinsically less stable than the larger, orange-red emitting particles. The biologically relevant pH region between 4 and 9 was tested (*i.e.*, pH $\approx$ 6–7 inside tumors and inflamed tissues; pH $\approx$ 5.5–6 in cellular compartments, including endosomes, and pH $\approx$ 4.5–5 in lysosomes),[18] various salt concentrations, the influence of micelle destroying surfactants,[19] such as sodium dodecyl sulfate (SDS) and dodecyl trimethyl ammonium bromide (DTAB), and strongly chelating ligands, such as ethylenediaminetetraacetic acid (EDTA). In Figure 5 the normalized quantum yield of QDs containing cross-linked micelles is plotted against time. The results document an outstanding stability of the micelles over 10 days. More detailed information can be seen in the Supporting Information, Figures S5 and S6 where the respective absorption and fluorescence spectra as well as

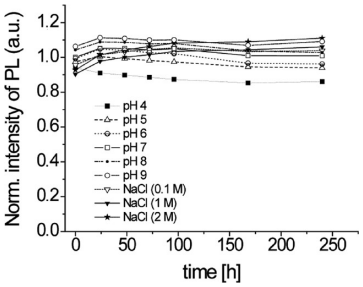

Figure 5. Normalized quantum yield of PI-*b*-PEO stabilized QDs in different media (pH 4−9, NaCl 0.1−2 M) over a period of 10 days.

the results of DLS measurements at different stages of aging are shown. An illustrative impression of the stability is seen in Supporting Information, Figure S7, where the respective samples after 10 days are shown under UV light. Additionally, a quantum dot solution in water was stored for three years on a laboratory shelf. The absorption and emission spectra showed almost no changes, except for a decrease in the fluorescence quantum efficiency by less than a factor of 2 (Supporting Information, Figure S8).

In summary, the particles were stable over the entire pH range and at high salt and moderate surfactant concentrations. Only a very high excess of surfactant and chelating molecules (10% SDS and 5% EDTA, corresponding to 600 000 and 300 000 molecules per nanoparticle, respectively) resulted in a drop in the fluorescence intensity. In the case of the surfactants, this was due to colloidal destabilization. It is noteworthy that the resulting nanoparticle precipitate could be completely redissolved in water after 10 days under full recovery of the fluorescence.

The comparison of PI-*b*-PEO−COOH stabilized QDs (emission max. 580 nm) in different aqueous media with commercial QDs from Life Technologies (Qdot585 ITK Carboxyl) and Cytodiagnostics (Trilite Fluorescent Nanocrystals 575 nm Carboxy) showed their outstanding stability even at lower pH values. The absorption and emission spectra at different times of storage are shown in Supporting Information, Figure S9. The particles of Cytodiagnostics (CY) precipitated within 2 h after incubation in PBS, pH 3 and 5. Same results were obtained with the particles of Life Technologies (LT). Just a small amount of QDs stayed in solution at pH 5. The PI-*b*-PEO particles stayed unaffected as the pictures of the solutions after 138 h of storage document (Figure 6). It has to be noted, that the LT particles are not spherical. Their oval shape leads to a form anisotropy, which effects the first absorption maximum. Thus, calculations of the QD concentration from absorption spectra lead to lower concentrations. We assume the concentration of these crystals much higher than specified.

Biological Applications. Prior to *in vitro* and *in vivo* targeting experiments, possible cell toxicity and nonspecific cell adhesion were investigated. The human

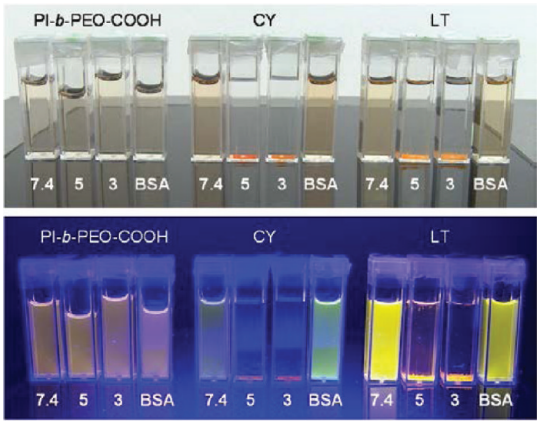

Figure 6. Pictures of PI-*b*-PEO−COOH stabilized QDs (emission max. 580 nm), QDs from Cytodiagnostics (Trilite Fluorescent Nanocrystals 575 nm Carboxy) (CY) and Life Technologies (Qdot585 ITK Carboxyl) (LT) after 138 h of incubation in PBS, pH 7.4, pH 5, pH 3, and in 1 w% BSA in PBS, pH 7.4. (Top) under daylight; (bottom) under UV excitation.

alveolar epithelial cell line A549 was used and treated with PI-*b*-PEO-X functionalized QDs and SPIOs (X = −OH and −COOH). Applying the well established water-soluble tetrazolium (WST8) and lactate dehydrogenase (LDH) toxicity assays, no toxic effects were found in the investigated concentration regime of 0.001 to 1 μM. This range represents a cell-to-QD ratio of 1 to 7.5 $\times$ 10^{10} up to 7.5 $\times$ 10^{13}. The corresponding plots with $CdCl_2$ as a reference can be seen in the Supporting Information (Figure S11. Note that here the particle concentrations are plotted, meaning that the total Cd load was higher by the agglomeration number of Cd within one particle, which was roughly 1000).

For the investigation of nonspecific cell adhesion, A549 cells were incubated for 50 min with 750 nM QD solutions (1:6.4 $\times$ 10^9 cell to particle ratio) followed by 4-fold lavage with phosphate buffered saline (PBS). The comparison of PI-*b*-PEO−COOH stabilized QDs with CY and LT particles *via* confocal laser scanning microscopy (Figure 7a) clarifies that the PI-*b*-PEO coating achieves the lowest degree of unspecific interaction. While CY and LT particles attach to and eventually transcend the cell-membrane, the PI-*b*-PEO particles could be removed by washing and no overall cell−particle interaction could be observed. It has to be mentioned though, that a statistically insignificant amount of cells showed unspecific cell−particle interaction (just one of the ~60 investigated cells, see Supporting Information, Figure S12). We have also investigated the cellular response on OH and COOH terminated PI-*b*-PEO particles after 17 h incubation time followed by a lavage. The corresponding confocal images are shown in Figure 7b. After that time an uptake is observable, which is stronger in the case of the COOH-terminated coating. Interestingly, no toxic effects were observable (Supporting Information, Figure S11) after same incubation times, indicating that the particle shell still

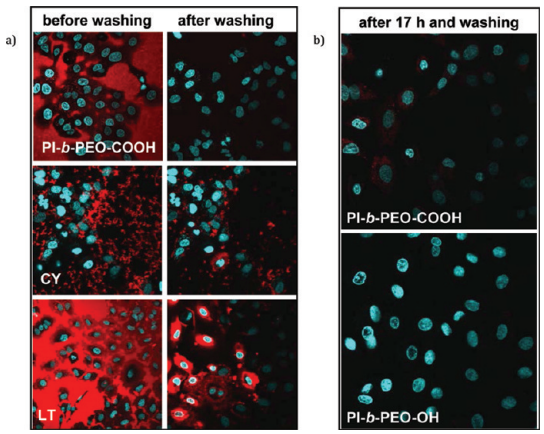

Figure 7. (a) Confocal microscope image of A549 cells incubated with 750 nM PI-*b*-PEO−COOH stabilized QDs, QDs from Cytodiagnostics (Trilite Fluorescent Nanocrystals 575 nm Carboxy) (CY) and Life Technologies (Qdot585 ITK Carboxyl) (LT) after an incubation time of 50 min. Red areas arise from QD fluorescence. The cells nuclei were counterstained with Hoechst 33342 (blue). Photoluminescence-intensity scans are shown in the Supporting Information (Figure S12) and verify that the fluorescence is due to the applied QDs. (Left) before washing; (right) after washing with PBS. (b) Confocal microscope images of A549 cells after QD-incubation for 17 h with subsequent washing. No uptake was observable for QDs stabilized by PI-*b*-PEO−OH polymers. PI-*b*-PEO−COOH stabilized QDs could be found in single cells. This suggests that the cellular uptake of nanoparticles is influenced by the cell cycle.

prevents direct contact or dissolution of the quantum dots and the cytosol. We also notice that uptake is not equal by all cells, that is, some show relative strong uptake and others almost none. This suggests that uptake might occur during cell proliferation (the cell cycle time of A549 cells is 40 h). Other authors also reported similar findings.[20] More detailed time-dependent investigations with a variety of terminating end groups are currently being performed in a high content screening device equipped with a life cell chamber and will be reported elsewhere. One should keep in mind that cell cycle times of healthy tissues are much longer than those from the cancer cell line A549. Thus, particle circulation times of *in vivo* experiments cannot be derived from these data.

In a further experiment 2×10^4 cells of the human melanoma cell line FEMX-I were incubated each with PI-*b*-PEO−COOH coated SPIOs, fluidMAG-PEG_{2000}/phosphate 50 nm (Chemicell GmbH), and Resovist (Bayer Schering Pharma). All SPIO particles had a hydrodynamic diameter of ~60 nm (according to DLS, intensity distribution). For all samples the applied amount of iron was varied between 200 and 400 μg. After 24 h the cells were washed with PBS and the cells were dissolved in Lysis Buffer and nitric acid. The amount of iron due to cellular adhesion and/or uptake by the cells was determined by flame atomic absorption spectrometry. A dependency of the applied iron amount with cellular adhesion/uptake could be determined for Chemicell and Resovist particles (Figure 8).

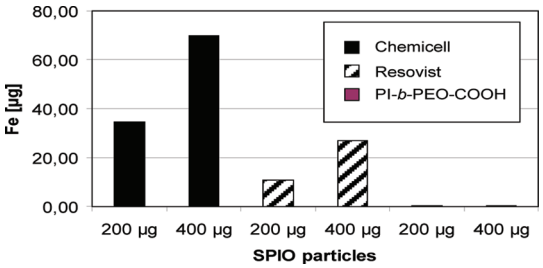

Figure 8. Average amount of iron for FemX-1 cells after incubation with Chemicell's fluidMAG-PEG_{2000}/phosphate 50 nm, Resovist, and PI-*b*-PEO stabilized SPIO nanoparticles for 24 h and 2-fold washing with PBS (3-fold determination). For each sample an amount of iron of 200 μg and 400 μg was used. The amount of iron of the cells was determined *via* flame atomic absorption spectrometry after dissolving the cells in nitric acid.

In the case of Chemicell particles 18% and in case of Resovist particles 6% of the applied iron could be found in the cells. In contrast, the PI-*b*-PEO−COOH stabilized particles show almost no cellular adhesion/uptake. The amount of iron was close to the detection limit.

Further the stability and changes of PI-*b*-PEO−COOH stabilized SPIOs were investigated in the presence of proteins by relaxivity measurements and DLS. Dilution series of the SPIO particles in ddH_2O, 3% BSA in PBS, pH 7.4, and pooled human blood plasma (BP), containing heparin and EDTA to inhibit coagulation, were prepared 24 h before the measurement was performed at 37 °C (physiological temperature) to ensure that the system had regained its adsorption equilibrium. The transverse relaxivity, r_2, was determined by measuring the characteristic relaxation at 1.41 T and plotting the inverse relaxation time against the ionic iron concentration. The slope of the as-determined straight line is defined as the relaxivity and represents the efficiency of the contrast agent.

The results for r_2 as well as the size of the micelles in the three media are shown in Figure 9. The experimental data shows only a slight increase in r_2 and no changes of their diameters, which demonstrates that these particles do not interact unspecifically and are suitable for biological applications.

PI-*b*-PEO encapsulated QDs were also incubated in ddH_2O, 1% BSA in PBS, pH 7.4. Neither change in the hydrodynamic diameter nor in the optical properties of QDs were observed by DLS and emission and absorption spectroscopy (see Supporting Information, Figure S10)

***In Vitro* Tests of Specific Targeting.** The biological functionality of antibody-coupled nanoconjugates was tested in cell culture experiments, before they were applied for *in vivo* studies. We focused on SPIO crystals, since their medical use as contrast agents has been already established. As a model system for specific targeting of tumor cells, the monoclonal antibody (mAb) T84.1 binding to carcinoembryonic antigen related cell adhesion molecules (CEACAM) and the

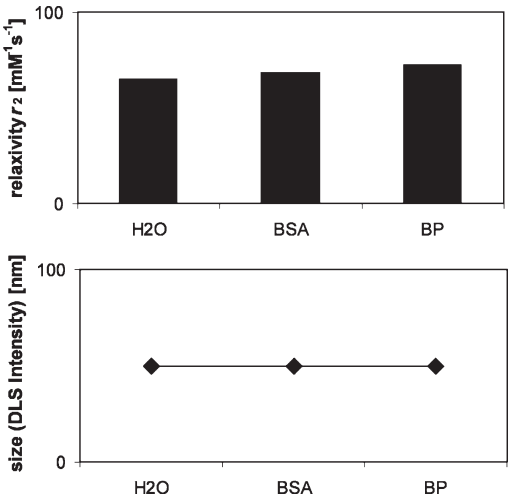

Figure 9. Size and transverse relaxivity, r_2, of PI-*b*-PEO–COOH stabilized SPIO nanoparticles in water, 3% BSA in PBS, pH 7.4, and pooled human blood plasma (BP) at 37 °C: (top) transverse relaxivity, r_2, at 1.41 T and 37 °C; (bottom) size determined by DLS (intensity).

CEACAM expressing FEMX-I were used. CEACAM are involved in intercellular adhesion and signal transduction events in a number of epithelia and are frequently dysregulated in carcinomas.

For the in the following presented MRI experiments, PI-*b*-PEO encapsulated iron oxide SPIOs with a hydrodynamic diameter of 50 nm were coupled to mAb T84.1 *via* EDC/sulfo-NHS coupling[21] (for details *cf.* Supporting Information). Cell suspensions of FEMX-I were incubated with T84.1-coupled nanoparticles without and with preincubation with nonbonded mAb T84.1 to block primary binding sites as a control for specific binding. After incubation for 30 min, the cells were washed and pelleted in Eppendorf tubes on a layer of polyacrylamide. Cellular probes underwent magnetic resonance imaging on a 3.0 T scanner using a small solenoid coil and a custom-made acrylic glass rack containing water. The T2-weighted images (Figure 10) demonstrate a distinct signal loss of the cell pellets incubated with T84.1-coupled nanoparticles and no significant signal loss for both controls, indicating less nonspecific binding. Similar results were also obtained using the HT29 cell line. The corresponding results are shown in the Supporting Information (Figure S13). These results showed the biological functionality of the antibody-coupled nanocomposites through the preservation of antibody affinity after coupling.

***In Vivo* Test of Specific Targeting.** To further prove the biological functionality, the antibody-coupled nanoparticles were tested in a xenografted mouse model of cancer. A sample of 10^6 FEMX-I cells was subcutaneously inoculated in the flank of four female C57Bl/6 severe combined immunodeficiency (SCID) mice. After 3 weeks of tumor growth, all mice developed well palpable subcutaneous tumors. T84.1-coupled as well as noncoupled nanoparticles as a control were

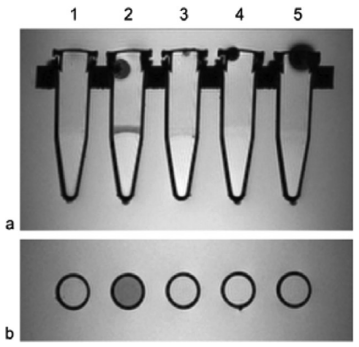

Figure 10. Magnetic resonance imaging of FEMX-I cell pellets after incubation with antibody-coupled nanocomposites using a T2 weighted coronal (a) and axial (b) turbo spin–echo sequence. Sample 1 contains PBS and sample 5 FEMX-I cells as control. A considerable signal decrease (darkening) of the cell pellet in sample 2 demonstrates detection of T84.1-coupled nanocomposites by MR imaging. Cells preincubated with nonbonded mAb T84.1 followed by incubation with T84.1-coupled nanocomposites in probe 3 as well as cells incubated with SPIOs without conjugated antibody in probe 4 show no signal decrease.

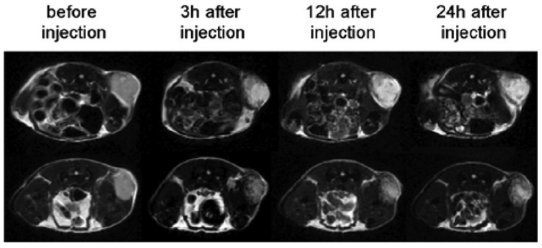

Figure 11. Magnetic resonance imaging of tumor-bearing mice (flanks at the pelvic level, n = 4) with a T2 weighted axial turbo spin–echo sequence. Three hours after injection of the uncoupled nanoparticles (upper row) and T84.1-coupled nanoparticles (lower row), diffuse hypointens (dark) areas especially in the well-vascularized outer rim of the tumors can be depicted in all mice, indicating a long circulation of the PI-*b*-PEO-coated particles. After 12 and 24 h, the outer parts of the tumors remain hypointens especially in the mouse treated with T84.1-coupled nanocomposites (lower row last image), indicating specific binding of the targeted SPIO. However, in the mice treated with uncoupled nanocomposites, minor unspecific accumulation of the contrast agent can be observed.

intravenously injected in the mice. Magnetic resonance imaging of the tumor-bearing mice was performed the day before as well as 3, 12, and 24 h after injection of the nanoparticles (Figure 11). Three hours after injection, all tumors showed a substantial signal loss of the tumor tissue in T2-weighted images, most likely due to a prolonged circulation time of the nanocomposites.

After 12 and 24 h, the distinct signal loss of the tumor periphery was preserved in mice treated with T84.1-coupled nanocomposites, indicating specific binding in the well-perfused outer tumor tissue. For further *in vivo* results consult Figure S14 (Supporting Information).

In another set of *in vivo* experiments with xenografted tumor models of the human melanoma cell line

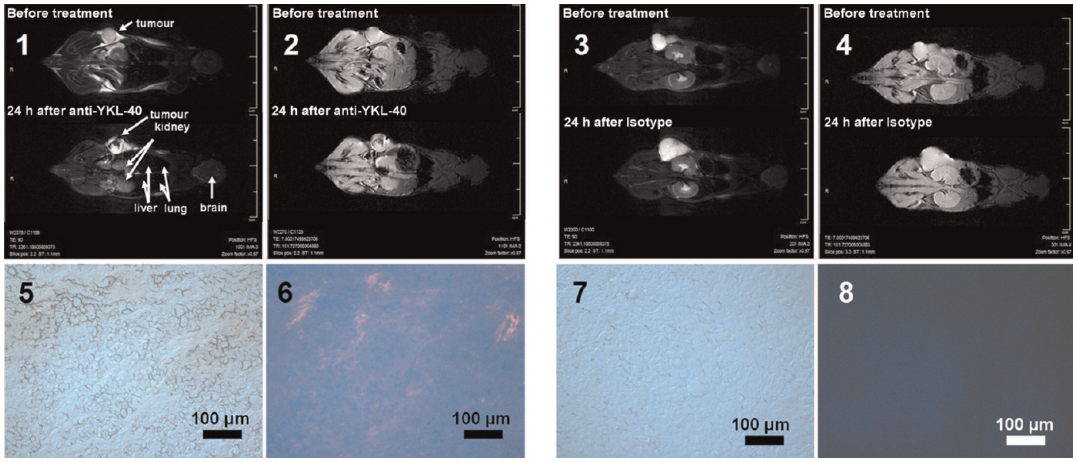

Figure 12. T2 (1) and T2* (2) weighted MR images of mice ($N = 3$) before (top) and after 24 h exposure (bottom) to anti-YKL-40-quantum dot and SPIO conjugates; (3, T2) and (4, T2*) show the corresponding images obtained with IgG isotype- conjugates; (5, 7) show microscope images (Normanski contrast) of the tumour tissue after exposure to the YKL-40 and the isotype antibody coupled nanocrystals, respectively; (6, 8) the corresponding fluorescence images (excitation at 365 nm).

LOX murine IgG2b κ, anti-YKL-40 antibodies and appropriate isotype control antibodies were coupled to CdSe/CdS/ZnS quantum dots and magnetite nanoparticles. We intravenously injected doses of 86 pmol constructed QD conjugates in combination with 300 pmol of SPIO-conjugates. Magnetic resonance imaging of tumor bearing mice was carried out before and 24 h after application of the antibody-conjugates (Figure12). In mice treated with the anti-YKL-40 antibody conjugates magnetic resonance imaging revealed a substantial signal loss of the tumor tissue in T2- and in the T2*-weighted images demonstrated in Figure12 parts 1 and 2 before injection (top) and after injection (bottom), whereas mice treated with isotype control conjugates did not reveal signal changes of the tumors shown in Figure12 parts 3 and 4. Histological analysis of tumors confirmed the presence of anti-YKL-40-QDs within the tumor tissue as demonstrated by confocal microscopy in Figure12 parts 5 (Normanski-contrast) and 6 (excitation at 365 nm), whereas isotype control QDs could not be detected in Figure12 parts 7 and 8. Notably, the strong MR signal decrease of tumors treated with anti-YKL-40 conjugates resulted from SPIO conjugates and partial hemorrhage, whereas histological sections demonstrate specifically that anti-YKL-40-QDs are in the vicinity of vessels assuming they bind to YKL-40 expressed by extracellular tumor matrix.

CONCLUSIONS

We have presented a versatile technique to biofunctionalize nanoparticles with surface affinity to amine groups, which includes nearly all inorganic nanocrystals relevant for molecular imaging. The coatings based on amphiphilic diblock-copolymers exhibit outstanding stability and inertness in the biological environment. The potential of this type of biolables could be demonstrated in tumor-specific MR imaging under *in vitro* and *in vivo* conditions.

METHODS

Preparation of Nanoparticles. Trioctylphosphine oxide (TOPO) capped CdSe/CdS/ZnS core−shell−shell nanoparticles were synthesized by methods reported previously.[22,23] The nanoparticles were precipitated twice with methanol to remove excess TOPO and stored in chloroform. FeOx nanoparticles, which were coated with sodium oleate, were obtained by a ultra-large-scale synthesis[24] and synthesized in high-boiling ether solvents.[25]

Synthesis of Polyisoprene (PI). The synthesis of PI was realized using dry argon as a cover gas. A 156 mL portion of isoprene (107 g, 1.57 mol) was purified in two steps in a cohesive glass apparatus, wherein the drying agent in the flasks were integrated and the isoprene was distilled from one flask to the next. First isoprene was dried with CaH_2 and after distillation in a second flask with di-*n*-butylmagnesium. In a final distillation step, it was transferred to a reactor containing 1.3 L of dried THF. As initiator, 30.0 mL of *sec*-butyllithium (1.30 mol/L, 39.0 mmol) was used. The reaction solution was stirred for 6 h at −60 °C. The polymerization was terminated with 4.00 mL (3.60 g, 82.0 mmol) of ethylene oxide to achieve hydroxyl end groups. After the addition of 5.00 mL of acetic acid (5.30 g, 87.0 mmol), the polymer was purified by precipitation in methanol.

Synthesis of Polyisoprene-*block*-poly(ethylene oxide) (PI-*b*-PEO) Block Copolymers. A 46.0 g portion of PI (11.0 mmol) was dissolved in 1.3 L of dry THF. Under an argon atmosphere, 110 mL of ethylene oxide (98.0 g, 2.22 mol) was purified in a three-step procedure. Ethylene oxide was dried with CaH_2, sodium mirror, and *n*-butyllithium. Finally it was distilled into the solution of PI in THF. A 9.00 mL portion of a solution of diphenylmethylpotassium (≈1 mol/L, 9.00 mmol) in cyclohexane was added. The solution was stirred 72 h at 40 °C and terminated with 4.00 mL of acetic acid (90.0 mmol). The PI-*b*-PEO was purified by precipitation in cold acetone.

Synthesis of PI-*b*-PEO−COOH. To 1.00 g of PI_{61}-*b*-PEO_{212}−OH (7.41×10^{-5} mol), dissolved in 10 mL of chloroform, 0.9 mg of the nucleophilic Steglich−Höfle catalyst 4-dimethylaminopyridine (DMAP) (7.41×10^{-6} mol, 0.1 equiv) were added. After the addition of 14.8 mg of succinic anhydride (1.48×10^{-4} mol, 2 equiv), dissolved in 3 mL of chloroform, the reaction mixture was stirred for 48 h at room temperature, concluding with the evaporation of the solvent and suspension of the yellow,

viscous pellet in a water and ethanol (3:2, 5 mL) mixture. The raw product was dialyzed for 2 days and lyophilized.

Synthesis of PI-N3 (PI-DETA). The polyisoprene polymer was equipped with 2,2′-diaminodiethylamine (DETA, -N3) by activation of the hydroxyl group of PI by a 20-fold excess of 1,1′-carbonyldiimidazol (CDI) in dry chloroform. After 14 h of stirring at room temperature, the excess of CDI was hydrolyzed by a 2-fold extraction the solution with 5 mL of water. Subsequently, the solution was dried with sodium sulfate. A 20-fold excess of N3 was added slowly to the solution. The reaction mixture was stirred for a further 12 h at a temperature of 55 °C. The product was precipitated twice in ethanol.

Ligand Exchange. The nanoparticles were incubated with a 300−600 molar excess of PI-N3. After 100 min, the nanoparticles were precipitated three times with ethanol or acetone out of chloroform. The nanoparticles were stored in chloroform.

Ligand Addition. The concentration of the PI_{30}-N3 coated nanoparticle/chloroform stock solution was defined by their UV−vis absorbance.[26] The dried particles were resuspended with a 50−500 times excess of PI-*b*-PEO ligands (primarily PI_{61}-*b*-PEO_{212}) in tetrahydrofuran (THF). AIBN (0.1 mg per 1 nmol particles) was added. After 10 min, the solution was injected into water, and the THF was removed in a nitrogen flow. After removal of the THF, the solution was heated at 70 °C for 60 min to initiate cross-link formation.

Stability Tests. In each case, 1.7×10^{-9} mol of the nanoparticles (QD to PI_{61}-*b*-PEO_{212}−OH ratio: 1 to 250) were dissolved in 3 mL of an aqueous solution containing surfactant (DTAB, and SDS) or NaCl or at different pH values (4−9).

Antibody Labeling. Carboxylic-functionalized nanoparticles were coupled with antibodies *via* the EDC/sulfo-NHS coupling strategy.[21]

Cytotoxicity Tests. For each assay A549 cells were plated at a density of 10^4 cells/mL in a 96-well plate and grown for a day before they were exposed to different concentrations of nanoparticles in DMEM + 10% Hepes Buffer. After 24 h incubation at a temperature of 37 °C in a humidified atmosphere containing 5% CO_2 LDH and WST-8 assays were prepared and measured according to BioVision Research Products (980 Linda Vista Ave, Mountain View, CA 94043 USA). The solutions were measured in a 96-well plate with a Infinite 2000 microplate reader (Tecan, Switzerland) at a wavelength of 460 nm. The reference wavelength was 620 nm.

Confocal Microscope Imaging. A549 cells (10000 cells per well) were grown for 2 days in Lab-Tek thin bottom chambers in DMEM medium containing 10% FCS. After a change of medium to DMEM + 10% Hepes buffer the nuclei of the cells were first counterstained with Hoechst 33342, and then the cells were exposed to the nanoparticles. They were observed immediately by confocal laser scanning microscopy (Olympus FluoViewTM FV1000 with an IX81 inverted microscope) as well as after several circles of washing using PBS buffer. For the 17 h-experiment cells were grown in Lab-Tek thin bottom chambers for 1 day before they were exposed to nanoparticles in DMEM + 10% Hepes buffer. After 17 h incubation at a temperature of 37 °C in a humidified atmosphere containing 5% CO_2, the cells were counterstained with Hoechst 33342 before they were observed by confocal laser scanning microscopy.

Incubation of Cells with SPIO Nanoparticles. A sample of 2×10^4 cells (per well) of the cell line FemX-1 was cultivated in 12-well plates (Nunclon Δ Surface, Nunc) using DMEM culture media (Gibco) w/10% FCS and 1% penicillin/streptomycin under 5% CO_2 atmosphere and 37 °C to about 70% confluence in each well. In every three wells nanoparticles with an iron oxide particle amount of either 200 and 400, dissolved in 1 mL DMEM media (+FCS, +pen/strept), were added. After 24 h incubation in 5% CO_2 atmosphere and 37 °C, the supernatant was removed and the wells were washed with 1 mL of PBS, pH 7.4. After the addition of 1 mL of cell dissociation buffer, enzyme-free, PBS-based (Gibco) and incubation for 24 h the cells were removed quantitatively and the wells were washed consequently with 500 μL nitric acid. The obtained lysates were heated up to 90 °C for 2 h in the present of 1:1 nitric acid to Lysis buffer. After determination of mass and density the iron concentration was determined *via* atomic absorption spectrometry.

Incubation of Cells for Cell Phantoms (*in Vitro* Experiments). Cells of the human melanoma cell line FEMX-I expressing the carcinoembryonic antigen related cell adhesion molecules (CEACAM) 1, 5, and 6 were trypsinized and washed three times in PBS. Cells were counted and split onto 12 round-bottom tubes with 1.9×10^7 cells in 500 μL of PBS supplemented with 1% BSA, respectively. Three samples were preincubated with unconjugated monoclonal antibody (mAb) T84.1 (10 μg/mL) for 15 min at 4 °C to block specific binding sites. Cell suspensions were then supplemented with T84.1-conjugated SPIOs (six tubes, whereas three were incubated with mAb) and unconjugated SPIOs (three tubes) at a dose of 50 μg/mL. Cells were incubated for 1 h at 4 °C. Afterward, cells were washed twice and resuspended in 300 μL of PBS.

MR Imaging of Cell Phantoms. Cell phantoms were prepared of 200 μL of polyacrylamide in 0.5 mL Eppendorf tubes. Cell suspensions were transferred in to the Eppendorf tubes and phantoms were kept 2 h at 4 °C for sedimentation. Cell phantoms were then examined on a 3.0 T magnetic resonance scanner (Intera, Philips, Best, The Netherlands) using a small solenoid receiver coil. Phantoms were placed in a custom-made device of acrylic glass contacting that fit into the receiver coil. The imaging protocol consisted of coronal and axial T2 turbo-spin echo (TSE) and T2* gradient echo (GRE) sequences.

For further information see Supporting Information.

Conflict of Interest: The authors declare no competing financial interest.

Acknowledgment. The authors thank the CAN GmbH for arranging the cytotoxicity tests and Dr. Neus Gomez Bastus for her support concerning TEM staining. Further, we thank Dr. Peter Nollau of the Department of Clinical Chemistry/Central Laboratories of the University and Medical Center Hamburg-Eppendorf for supplying the T84.1 antibodies. Furthermore, U. Tromsdorf for the supply of the iron oxide nanoparticles for the cell phantoms and Dr. V. Sinnwell from the Institute of Organic Chemistry for the NMR measurements are acknowledged. This work was supported by grants from the European Union's Seventh Framework Programme for the *In Vivo* Imaging of Beta-Cell Receptors by Applied Nano Technology project (VIBRANT, FP7-228933-2), the State Excellence Initiative for the Nanotechnology in Medicine cluster, and from the Bundesministerium für Bildung und Forschung for the Tailored Magnetic Nanoparticles for Cancer Targeting project (TOMCAT, 01 EZ 0824).

Supporting Information Available: Complete refs 11 and 25, analytical instruments, experimental procedures for polymer synthesis, phase transfer of nanoparticles, stability tests, absorption and emission spectra, cytotoxicity tests, further *in vitro* and *in vivo* experiments and additional experimental data. This material is available free of charge *via* the Internet at http://pubs.acs.org.

REFERENCES AND NOTES

1. Smith, A. M.; Duan, H.; Rhyner, M. N.; Ruan, G.; Nie, S. A Systematic Examination of Surface Coatings on the Optical and Chemical Properties of Semiconductor Quantum Dots. *Phys. Chem. Chem. Phys.* **2006**, *8*, 3895–3903.
2. Hyeon, T.; Lee, S. S.; Park, J.; Chung, Y.; Na, H. B. Synthesis of Highly Crystalline and Monodisperse Maghemite Nanocrystallites without a Size-Selection Process. *J. Am. Chem. Soc.* **2001**, *123*, 12798–12801.
3. Talapin, D. V.; Mekis, I.; Goetzinger, S.; Kornowski, A.; Benson, O.; Weller, H. CdSe/CdS/ZnS and CdSe/ZnSe/ZnS Core−Shell−Shell Nanocrystals. *J. Phys. Chem. B* **2004**, *108*, 18826–18831.
4. Medintz, I. L.; Uyeda, H. T.; Goldman, E. R.; Mattoussi, H. Quantum Dot Bioconjugates for Imaging, Labelling and Sensing. *Nat. Mater.* **2005**, *4*, 435–446.
5. Michalet, X.; Pinaud, F. F.; Bentolila, L. A.; Tsay, J. M.; Doose, S.; Li, J. J.; Sundaresan, G.; Wu, A. M.; Gambhir, S. S.; Weiss, S. Quantum Dots for Live Cells, *in Vivo* Imaging, and Diagnostics. *Science* **2005**, *307*, 538–544.

6. Chan, W. C. W.; Nile, S. Quantum Dot Bioconjugates for Ultrasensitive Nonisotopic Detection. *Science* **1998**, *281*, 2016–2018.
7. Patolsky, F.; Gill, R.; Weizmann, Y.; Mokari, T.; Banin, U.; Willner, I. Lighting-Up the Dynamics of Telomerization and DNA Replication by CdSe–ZnS Quantum Dots. *J. Am. Chem. Soc.* **2003**, *125*, 13918–13919.
8. Xu, C.; Xu, K.; Gu, H.; Zheng, R.; Liu, H.; Zhang, X.; Guo, Z.; Xu, B. Dopamine as A Robust Anchor to Immobilize Functional Molecules on the Iron Oxide Shell of Magnetic Nanoparticles. *J. Am. Chem. Soc.* **2004**, *126*, 9938–9939.
9. Xie, J.; Xu, C.; Xu, Z.; Hou, Y.; Young, K. L.; Wang, S. X.; Pourmond, N.; Sun, S. Linking Hydrophilic Macromolecules to Monodisperse Magnetite (Fe_3O_4) Nanoparticles *via* Trichloro-s-triazine. *Chem. Mater.* **2006**, *18*, 5401–5403.
10. Kingshott, P.; Griesser, H. J. Surfaces That Resist Bioadhesion. *Curr. Opin. Solid State Mater. Sci.* **1999**, *4*, 403–412.
11. Bruns, O. T; Ittrich, H.; Peldschus, K.; Kaul, M. G.; Tromsdorf, U. I.; Lauterwasser, J.; Nikolic, M. S.; Mollwitz, B.; Merkel, M.; Bigall, N. C.; *et al*. Real-Time Magnetic Resonance Imaging and Quantification of Lipoprotein Metabolism *in Vivo* using Nanocrystals. *Nat. Nanotechnol.* **2009**, *4*, 193–201.
12. Pöselt, E.; Fischer, S.; Förster, S.; Weller, H. Highly Stable Biocompatible Inorganic Nanoparticles by Self-Assembly of Triblock-Copolymer Ligands. *Langmuir* **2009**, *25*, 13906–13913.
13. Al-Jarrah, M. M. F.; Apikian, R. L.; Ahmed, E. Living Polymerization. *Polym. Bull.* **1984**, *12*, 433–436.
14. De Vringer, T.; Joosten, J. G. H.; Junginger, H. E. A Study of the Hydration of Polyoxyethylene at Low Temperatures by Differential Scanning Calorimetry. *Colloid Polym. Sci.* **1986**, *264*, 623–630.
15. Roberts, M. J.; Bentley, M. D.; Harris, J. M. Chemistry for Peptide and Protein PEGylation. *Adv. Drug Delivery Rev.* **2002**, *54*, 459–476.
16. Thompson, M. S.; Vadala, T. P.; Vadala, M. L.; Lin, Y.; Riffle, J. S. Synthesis and Applications of Heterobifunctional Poly(ethylene oxide) Oligomers. *Polymer* **2008**, *49*, 345–373.
17. Zalipsky, S. Functionalized Poly(ethylene glycols) for Preparation of Biologically Relevant Conjugates. *Bioconjugate Chem.* **1995**, *6*, 150–165.
18. Yang, Q.; Wang, S.; Fan, P.; Wang, L.; Di, Y.; Lin, K.; Xiao, F.-S. pH-Responsive Carrier System Based on Carboxylic Acid Modified Mesoporous Silica and Polyelectrolyte for Drug Delivery. *Chem. Mater.* **2005**, *17*, 5999–6003.
19. Pispas, S.; Hadjichristidis, N. Aggregation Behavior of Poly(butadiene-*b*-ethylene oxide) Block Copolymers in Dilute Aqueous Solutions: Effect of Concentration, Temperature, Ionic Strength, and Type of Surfactant. *Langmuir* **2003**, *19*, 48–54.
20. Kim, J. A.; Åberg, C.; Salvati, A.; Dawson, K. A. Role of Cell Cycle on the Cellular Uptake and Dilution of Nanoparticles in a Cell Population. *Nat. Nanotechnol.* **2012**, *7*, 62–68.
21. Grabarek, Z.; Gergely, J. Zero-Length Crosslinking Procedure with the Use of Active Esters. *Anal. Biochem.* **1990**, *185*, 131–135.
22. Mekis, I.; Talapin, D. V.; Kornowski, A.; Haase, M.; Weller, H. One-Pot Synthesis of Highly Luminescent CdSe/CdS Core–Shell Nanocrystals *via* Organometallic and "Greener" Chemical Approaches. *J. Phys. Chem. B* **2003**, *107*, 7454–7462.
23. Talapin, D. V.; Rogach, A. L.; Kornowski, A.; Haase, M.; Weller, H. Highly Luminescent Monodisperse CdSe and CdSe/ZnS Nanocrystals Synthesized in a Hexadecylamine–Trioctylphosphine Oxide–Trioctylphospine Mixture. *Nano Lett.* **2001**, *1*, 207–211.
24. Park, J.; An, K.; Hwang, Y.; Park, J.-G.; Noh, H.-J.; Kim, J.-Y.; Park, J.-H.; Hwang, N.-M.; Hyeon, T. Ultra-Large-Scale Syntheses of Monodisperse Nanocrystals. *Nat. Mater.* **2004**, *3*, 891–895.
25. Tromsdorf, U. I.; Bigall, N. C.; Kaul, M. G.; Bruns, O. T.; Nikolic, M. S.; Mollwitz, B.; Sperling, R. A.; Reimer, R; Hohenberg, H.; Parak, W. J.; *et al*. Size and Surface Effects on the MRI Relaxivity of Manganese Ferrite Nanoparticle Contrast Agents. *Nano Lett.* **2007**, *7*, 2422–2427.
26. Allgaier, J.; Poppe, A.; Willner, L.; Richter, D. Synthesis and Characterization of Poly[1,4-isoprene-*b*-(ethylene oxide)] and Poly[ethylene-*co*-propylene-*b*-(ethylene oxide)] Block Copolymers. *Macromolecules* **1997**, *30*, 1582–1586.